Acta Crystallographica Section A
Foundations of Crystallography
ISSN 0108-7673

Received 6 July 2009
Accepted 23 October 2009

Dense quasicrystalline tilings by squares and equilateral triangles

Michael O'Keeffe* and Michael M. J. Treacy

Department of Chemistry and Biochemistry, and Department of Physics, Arizona State University, Tempe, AZ 85287, USA. Correspondence e-mail: mokeeffe@asu.edu

Dense square-symmetry tilings of the plane by equilateral triangles and squares are described. Repeated substitution of a vertex of a tiling by groups of vertices leads asymptotically to a limiting density that is independent of the starting pattern and to a family of quasicrystalline patterns with 12-fold symmetry. Diffraction patterns were computed by treating the vertices as point scatterers. As the number of substitutions increases, and as the unit-cell size increases, the diffraction patterns from a single unit cell develop a near-perfect 12-fold symmetry. In addition, the low-intensity background scattering in the diffraction patterns exhibits fractal-like self-similar properties, with motifs of local intensity recursively decorating the more intense features as the number of substitutions progresses.

In a review (O'Keeffe & Hyde, 1980) of 2-periodic nets relevant to crystal chemistry, it was remarked of a certain net that '. . . this is the densest net with square symmetry that we have discovered'. 'Densest' refers to the structure considered as a packing of equal circles and density is measured as the number of unit-diameter circles per unit area. The fraction of the plane covered by these circles is this density multiplied by $\pi/4$. Here we describe a series of denser circle packings with square symmetry. These patterns also correspond to tiling the plane by squares and equilateral triangles.

The simplest square packing of equal circles has circle centers on a 4^4 net and has density 1.0, but a denser one with all circles related by symmetry has centers on a $3^2.4.3.4$ net (Fig. 1); this latter has density $4/(2+\sqrt{3}) = 1.07180$.

The structure referred to by O'Keeffe & Hyde (1980) is obtained by replacing each circle of a 4^4 packing by a group of 19 circles with centers on, or inside, a dodecagon as shown in Fig. 1(*c*) to produce the packing **suv** shown in Fig. 2. To maintain square symmetry it can only be done in the way shown in the figure and the symmetry is now *p*4*gm*. This packing has density $15/(7+4\sqrt{3}) = 1.07695$. But it is clear that the same operation carried out on a $3^2.4.3.4$ packing will produce a denser structure, again with symmetry *p*4*gm*. There are two ways of doing this and the resultant patterns are symbolized **esq** and **esr**. These have density $56/(26+15\sqrt{3}) = 1.07732$. The nets of these three structures may be found in the RCSR database at http://rcsr.anu.edu.au (O'Keeffe *et al.*, 2008). That source will provide coordinates and other crystallographic data.

However, there is no reason to stop at this point. Individual circles of the sphere packings of Fig. 2 can be again replaced by the 19-circle motif in a way that preserves the symmetry, and this substitution tiling process repeated *ad infinitum*. The density of the structures is determined by counting squares and triangles. If at the nth iteration there are t_n triangles and s_n squares, then at the next iteration

$$\begin{aligned} t_{n+1} &= 7t_n + 16s_n, \\ s_{n+1} &= 3t_n + 7s_n. \end{aligned} \tag{1}$$

Each square of unit area is associated with one vertex (or equivalently, four 1/4-vertices at each corner), and each

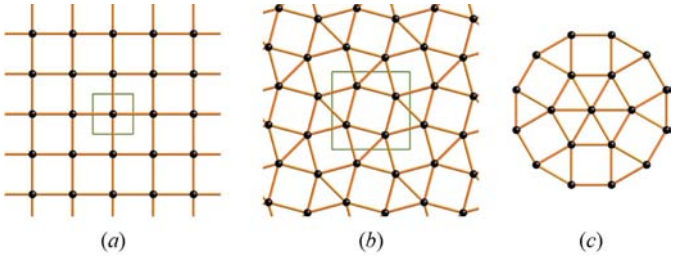

Figure 1
(*a*) The centers of a circle packing based on 4^4. (*b*) The centers of a circle packing based on $3^2.4.3.4$. (*c*) Circle centers of a dodecagonal unit of 19 circles.

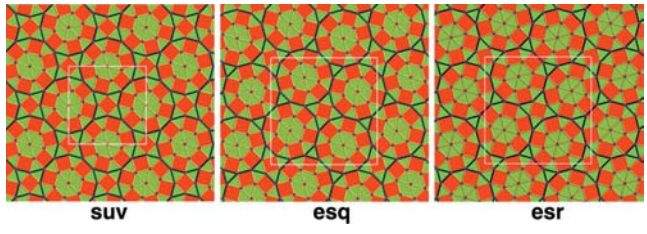

Figure 2
From left: **suv**, the pattern derived by replacing the centers of a 4^4 circle packing by the units of Fig. 1(*c*). **esq** and **esr**, two square-symmetry patterns derived by replacing the centers of a $3^2.4.3.4$ circle packing by the units of Fig. 1(*c*). A unit cell is outlined in every case.

triangle of area $\sqrt{3}/4$ is associated with half of a vertex (three 1/6-vertices).

The density ρ_n (number of vertices per unit area), after iteration n, is then

$$\rho_n = \frac{s_n + t_n/2}{s_n + \sqrt{3}t_n/4} = \frac{1 + t_n/2s_n}{1 + \sqrt{3}t_n/4s_n}. \quad (2)$$

The density therefore depends on the ratio t_n/s_n. For any positive and finite starting value of t_1 and s_1, the ratio converges rapidly so that in the limit of infinite n, $t_{n+1}/s_{n+1} = t_n/s_n = t_\infty/s_\infty = 4/\sqrt{3}$. This ratio is confirmed by examining the eigenvectors of the generating matrix (1) in the limit $n \rightarrow \infty$. When this is done, a second solution is found, $t_\infty/s_\infty = -4/\sqrt{3}$. Taking the positive solution, we find that the limiting density ρ_∞ tends to the same finite value regardless of the starting configuration,

$$\rho_\infty = 1/2 + 1/\sqrt{3} = 1.07735\ldots. \quad (3)$$

This is exactly the average of the densities of 4^4 and 3^6 (the densest circle packing). The second, negative, solution gives an infinite density for all starting configurations, and does not correspond to a physically meaningful tiling.

The two eigenvalues of the substitution matrix in (1) are $(2 \pm \sqrt{3})^2$, the larger value corresponding to the scaling of the growing structure. Thus, after each substitution step, the number of vertices per unit cell grows by a factor $(2 + \sqrt{3})^2 \simeq 13.928$, and the unit-cell edge lengthens by a factor $2 + \sqrt{3} \simeq 3.7320$. The smaller eigenvalue, $(2 - \sqrt{3})^2 \simeq 0.07180$, suggests a shrinking structure and, as pointed out above, does not correspond to a physically meaningful tiling.

There are infinitely many circle packings with square symmetry and with the circle centers at the vertices of a tiling of the plane by equilateral triangles and squares and, as explained below, infinitely many different circle packings with this limiting density. It is clear, however, that there are denser square circle packings. For example, one may take an arbitrarily large fragment of 3^6, with close to square shape, and repeat those about a point with $p4$ symmetry. In the limit of very large fragments the density will approach that of 3^6, although the 'grain boundaries' between the four fragments of 3^6 will inevitably be incommensurate non-close-packed structures. However, if we restrict the discussion to edge-to-edge tilings by equal-sided squares and equilateral triangles, we suspect that the structures we describe are the densest with square symmetry.

It must be mentioned that our 'inflation rule' of replacing a vertex by a set of 19 vertices has been used earlier in different deterministic contexts by Stampfli (1986) and by Schlottmann (as described by Hermisson *et al.*, 1997; see also Zeng & Ungar, 2006). The density of squares and triangles for such an inflated structure was earlier derived by Leung *et al.* (1988).[1]

We have investigated iterations of **esq** in some detail. There are two ways of replacing a vertex with a cluster of vertices (the two ways are related by a 30° rotation). The **esq** pattern has nine kinds of vertex and a total of 56 in the unit cell so there are $2^9 = 512$ ways of producing the next generation while maintaining square symmetry, and 2^{56} ways ignoring symmetry. We took just one of the 512 square patterns as **esq2**; from this we took arbitrarily one new square pattern **esq3** (Fig. 3) and from that one square pattern to form **esq4**. At this point there are 19003 kinds of vertex and $2^{19003} \simeq 10^{4720}$ ways of making **esq5**. This is still an almost vanishingly small fraction of the $2^{151316} \simeq 10^{45551}$ ways of making the next generation regardless of symmetry, so the square-symmetry patterns are special. The patterns can be viewed in two ways. We can consider the periodic ($p4gm$) patterns as successive approximants to a quasiperiodic structure, or we can consider the unit cell itself as an increasingly large finite fragment of a quasiperiodic structure. We consider the latter.

Diffraction patterns can be calculated in the usual way by summing over all the pairwise interference terms between scatterers in the unit cell, which here are located at the vertices of the tiling. Although there is no periodicity within the unit cell, the location of all of the scatterers is well defined.

For simplicity, we start with a primitive initial cell that contains one copy of our substitution pattern. The Fraunhofer diffracted wavefunction is simply

$$\psi(\mathbf{Q}) = \sum_{m=1}^{N} f_m(\mathbf{Q}) \exp(-i\mathbf{Q} \cdot \mathbf{r}_m) \quad (4)$$

where $f_m(\mathbf{Q})$ is the atomic scattering factor at wavevector $\mathbf{Q}$. The sum is over the atoms in the unit cell, which in this instance are the N atoms in the substitution pattern.

Now we substitute each of these vertices with a new copy of the substitution pattern. To accomplish this we must first expand the model by a factor s (in our case, $s = 2 + \sqrt{3}$), then we replace each vertex with a copy of the substitution pattern. It may be necessary to rotate the pattern relative to the original orientation of the set of coordinates $\{\mathbf{r}_m\}$. This is achieved by applying a rotation operation $\mathbf{R}$ before substituting. In our case any angle that is a multiple of 30° in the plane is allowed (0° and 30° generate different structures). Thus, the new coordinate set is generated by

$$\{\mathbf{r}_{m'}\} \equiv \sum_{m=1}^{N} \left(s\mathbf{r}_m + \sum_{n=1}^{N} \mathbf{R}\mathbf{r}_n\right). \quad (5)$$

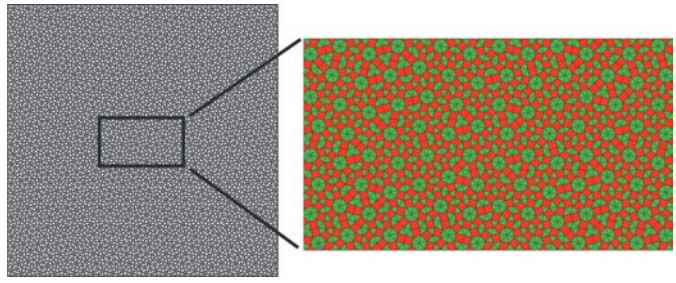

Figure 3
Section taken from the unit cell of **esq3**, showing the fourfold rotation axis at the center, but the absence of translational symmetry within the unit cell.

[1] We are grateful to a referee for calling our attention to this work, of which we were unaware at the time the present work was completed.

The diffracted wavefunction after this expansion/decoration step is now

$$\psi(\mathbf{Q}) = \sum_{m=1}^{N} \exp(-is\,\mathbf{Q}\cdot\mathbf{r}_m) \sum_{n=1}^{N} w_n f_n(\mathbf{Q}) \exp(-i\mathbf{Q}\cdot\mathbf{R}\mathbf{r}_n). \quad (6)$$

The weighting (or occupancy) factor w_n accounts for the situation in which multiple degenerate copies of the same scatterer are generated at a particular location $\boldsymbol{r}_n$. A second substitution expands the set of coordinates to

$$\{\mathbf{r}_{m'}\} \equiv \sum_{m=1}^{N} \Big[s^2\mathbf{r}_m + \sum_{\nu=1}^{N} \big(s\mathbf{R}\mathbf{r}_m + \sum_{q=1}^{N} \mathbf{R}^2\,\mathbf{r}_q\big)\Big] \quad (7)$$

and the diffracted wavefunction is now

$$\psi(\mathbf{Q}) = \sum_{m=1}^{N} \exp(-is^2\mathbf{Q}\cdot\mathbf{r}_m) \times \sum_{n=1}^{N} w_n f_n(\mathbf{Q}) \exp(-is\mathbf{Q}\cdot\mathbf{R}\mathbf{r}_n) \times \sum_{q=1}^{N} w_q f_q(\mathbf{Q}) \exp(-i\mathbf{Q}\cdot\mathbf{R}^2\mathbf{r}_q). \quad (8)$$

If this expansion/convolution is repeated, the Fraunhofer diffracted wavefunction $\psi_M(\mathbf{Q})$ after the Mth generation can be expressed as the product

$$\psi_M(\mathbf{Q}) = \prod_{p=1}^{M} \varphi_p(\mathbf{Q}), \quad (9)$$

where

$$\varphi_p(\mathbf{Q}) = \sum_{m=1}^{N} F_m^{(pM)} \exp\big(-is^{M-p}\,\mathbf{Q}\cdot\mathbf{R}^{p-1}\mathbf{r}_m\big). \quad (10)$$

Since the rotation of points in space is equivalent to a contravariant rotation of the reciprocal-lattice vector by the transpose of $\mathbf{R}$, that is $\widetilde{\mathbf{R}}$, we can rewrite $\varphi_p(\mathbf{Q})$ as

$$\varphi_p(\mathbf{Q}) = \sum_{m=1}^{N} F_m^{(pM)} \exp\big[-i\big(s^{M-p}\widetilde{\mathbf{R}}^{1-p}\mathbf{Q}\big)\cdot\mathbf{r}_m\big]. \quad (11)$$

This form shows that we can interpret the expansion and rotation of coordinates in real space at each generation step, as a shrinking and contrarotation of the reciprocal-lattice vectors $\mathbf{Q}$ in reciprocal space relative to the vectors at the previous step. Thus, each generation potentially produces a fractal-like self-similar contribution to the diffraction pattern. The scattering factor $F_m^{(pM)}$ is unity for all terms except the final generation $p = M$ when the iterative generation of points is ended and the scatterers themselves are finally realised. Thus

$$F_m^{(pM)} = \begin{cases} 1 & \text{if } p \neq M, \\ w_m f_m(\mathbf{Q}) & \text{if } p = M. \end{cases} \quad (12)$$

As before, the weighting (or occupancy) factor w_m compensates for degenerate copies of the same scatterer at location $\boldsymbol{r}_m$.

The above analysis leads us to expect diffraction patterns with fractal-like self-similar properties. In practice, the application of equations to compute the diffraction pattern is cumbersome. Since it is straightforward to compute the coordinates of all the scatterers in the unit cell at each generation, we computed the Fraunhofer diffracted wavefield $\psi_M(\mathbf{Q})$ directly by explicitly calculating the interference terms for the whole cell after the Mth generation. The diffracted intensity is then $|\psi_M(\mathbf{Q})|^2$.

The diffracted intensity from a single unit cell of the **esq** structure (Fig. 4*a*), which contains 112 vertices, shows well defined peaks with an apparent 12-fold symmetry. Close inspection of the weak background scattering shows that the 12-fold symmetry is not perfect, and that the true symmetry is fourfold. The diffraction pattern from the infinite lattice (not shown) is markedly different, exhibiting a clear fourfold axis consistent with space group $p4gm$ for the unit-cell dimensions of **esq**. The pattern from a single unit cell (Fig. 4*a*) is the form factor that is applied to the pattern from the primitive lattice.

The structure arising from the second generation, here referred to as **esq2**, contains 780 atoms. Its diffraction pattern (Fig. 4*b*) develops sharper peaks and already has a near-perfect 12-fold symmetry. The sharp peaks occur at non-integer reciprocal-lattice vectors. The reciprocal-lattice vectors of the periodic versions of these structures shrink in magnitude by the factor $2 + \sqrt{3}$ with each generation. Since we are examining the form factors for the scattering from a single unit cell, we label the peaks in terms of reciprocal edge units (nearest-neighbor inter-vertex distance). The peak labeled pq in Fig. 4*b* is located at approximately (1.5, 1.5) reciprocal edge. Again, the 12-fold symmetry exhibited by the intense sharp peaks is violated in subtle ways by the background intensity. The patterns for the next three generations, **esq3** (Fig. 4*c*), **esq4** (Fig. 4*d*) and **esq5** (Fig. 4*e*), closely resemble that for **esq2**. The most intense peaks in these patterns can be seen in Fig. 4(*f*), which is the same pattern as Fig. 4(*c*) for **esq4**, but with the intensity scale reduced by three orders of magnitude.

The numbers of vertices in each unit cell after each generation are 10 864, 151 316 and 2 888 456, respectively. Although there is no obvious relationship between the strongly diffracted intensity and density of the structure, when the intensity scale is increased so that some of the background intensity is visible (as shown in Figs. 4*c*–4*e*) subtle differences appear.

These differences can be seen in Fig. 5, which shows the intensity region in the neighborhood of the $p, q \simeq (1.5, 1.5)$ peak. The pattern for **esq3** (Fig. 5*b*) is displayed at the same reciprocal-lattice scale as for **esq2** (Fig. 5*a*). Already self-similar features are appearing. In the upper left of the **esq3** pattern a sharp spot emerges that is a smaller, but strikingly similar, version of the pattern at pq for **esq2**. Even more striking is when we generate the **esq4** pattern (Fig. 5*c*) we see that there is a near-perfect copy of the **esq3** pattern decorating the same pq spot, but shrunk by the factor $s = 2 + \sqrt{3} \simeq 3.732051\ldots$. To emphasize the similarity, Fig. 5(*d*) shows the **esq4** pattern expanded by this factor. Comparison with the **esq3** pattern in Fig. 5(*b*) emphasizes the similarity. The main reason why the patterns are not perfectly self-similar is because the intensity of the sharp spots grows approximately as the square of the number of vertices, that is as $\sim s^4$, whereas the intensity of each new manifestation of the motif grows in

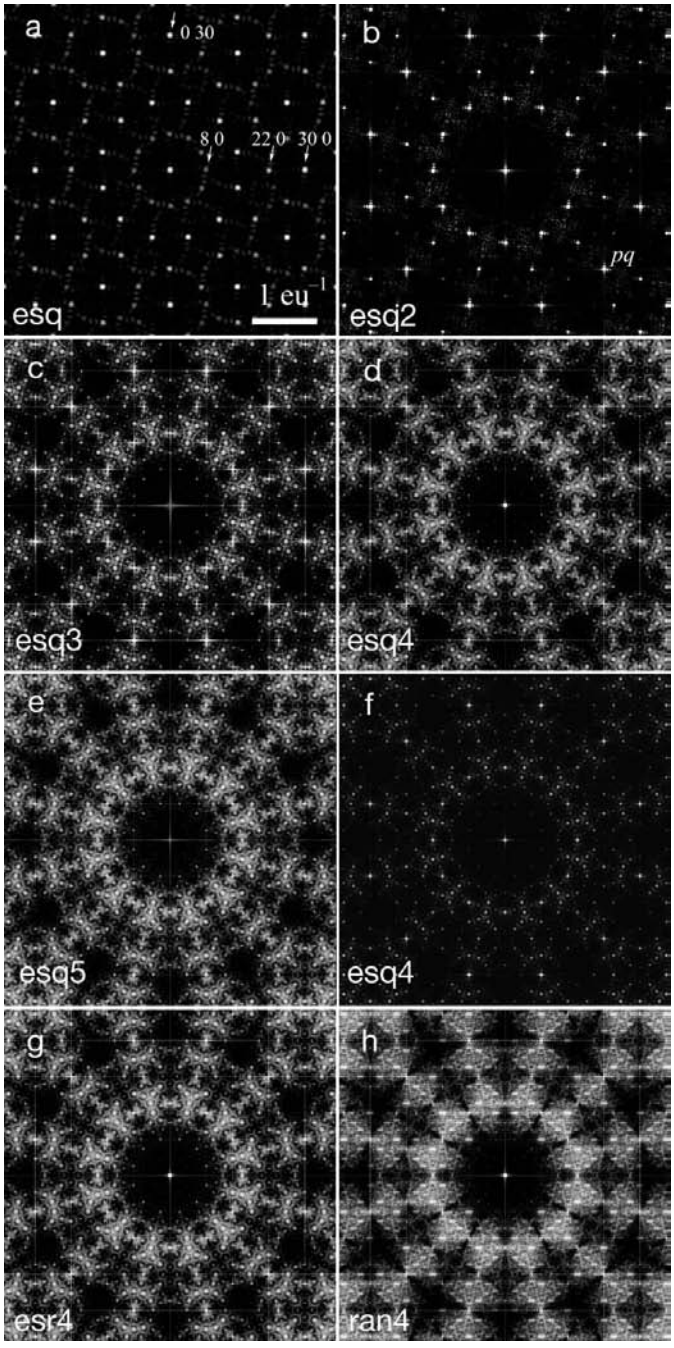

Figure 4
(*a*)–(*e*) Kinematical diffraction intensities from a single unit cell of five generations based on the **esq** structure. The scale marker in (*a*) is the same for all patterns and is in reciprocal edge units (eu^{-1}). The indices in (*a*) are relative to the unit cell. The sharp peaks labeled *pq* in (*b*) are centered at irrational indices near (1.5, 1.5) eu^{-1}. The intensity surrounding each *pq* peak becomes more elaborate with each generation exhibiting some self-similar features. As the generation number increases, the pattern approaches perfect 12-fold rotation symmetry. (*f*) The diffraction pattern for **esq4** (as in *d*), but with the intensity scale decreased by three orders of magnitude so that only the most intense peaks appear. (*g*) The equivalent diffraction intensity for the fourth generation of the **esr** variant, **esr4**. It closely resembles **esq4**. (*h*) The equivalent diffraction intensity for the fourth generation of the randomized tiling **ran4**. There is a significant increase in diffuse intensity compared with **esq4** and **esr4**. The symmetry is reduced to fourfold.

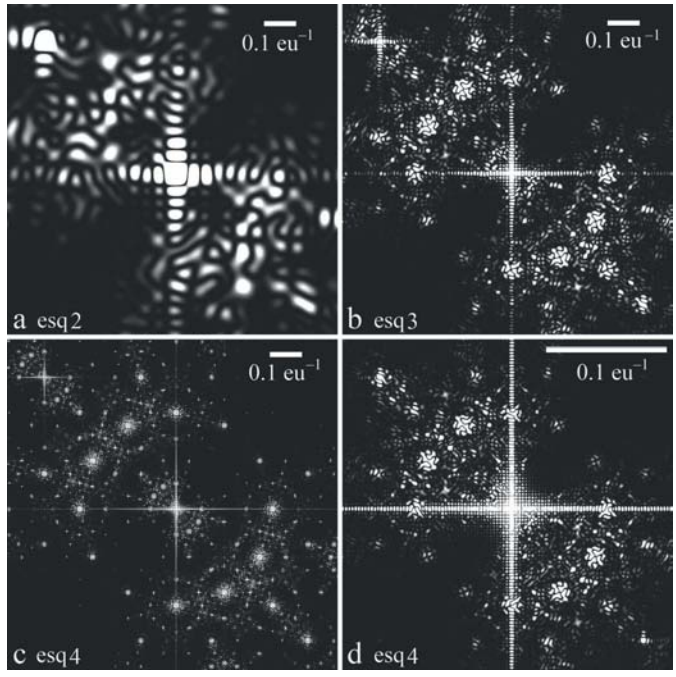

Figure 5
Detailed views of the Fourier transforms of (*a*) **esq2**, (*b*) **esq3** and (*c*) **esq4** circle packings, centered at the reciprocal-lattice point *pq* near (1.5, −1.5) eu^{-1} as indicated in Fig. 4(*b*). (*d*) The central region of (*c*) magnified by a factor of $2 + \sqrt{3} = 3.73205$, and at the same intensity scaling, showing the strong similarities to the pattern from the previous iteration, shown above it in (*b*). The intensities in (*b*) and (*c*) have each been scaled down successively by a factor $(2 + \sqrt{3})^2 = 13.93$ relative to (*a*). Comparison of (*b*) and (*d*) suggests that the intensity of the fractal decoration grows linearly with the number of atoms, whereas the intensity of the sharp peaks, once they have appeared, subsequently grows superlinearly, approaching the square of the number of atoms.

proportion to the number of vertices, or $\sim s^2$. Consequently, the shoulders of the bright peaks eventually dominate the background scattering.

With each generation, the pattern from each single unit cell better approximates perfect 12-fold symmetry. Also the sharp spots occur near irrational *pq* values.

The patterns are very similar for the **esr** sequence of structures. The pattern for **esr4** (Fig. 4*g*) is superficially identical to that for **esq4** (Fig. 4*d*). However, the background intensities show subtle differences. The diffraction pattern for a fourth-generation structure, **ran4**, built by randomly orienting the 19-atom motif by 0° or 30° before placing in position, is substantially different from the ordered patterns (Fig. 4*h*). Strong diffuse background intensity is generated, and none of the fractal-like behavior emerges. Strictly, the label **ran** does not refer to a unique structure, but instead represents a vast family of possible structures, of which we examine just one. However, all random conformations with approximately half of the motifs rotated should give similar strong features in the diffraction patterns. The differences will only appear in the subtle details of the diffuse scattering.

Each generation expands the unit-cell size by $\sim s \simeq 3.732$, and the number of vertices per unit cell increases by a factor $\sim s^2 \simeq 13.93$. After four additional generations applied to the

esq net, there are almost three million vertices. After about 20 generations, a (plane) unit cell with approximately one mole of vertices will be generated. For all practical purposes, such a single cell approximates an infinite structure. In this limit, our nets constitute space-filling aperiodic tilings of squares and equilateral triangles. In common with quasicrystals (Gähler & Klitzing, 1997), the diffraction patterns exhibit sharp spots with irrational *pq* indices and have rotational symmetry that is not supported by periodic plane groups. In our case, we have 12-fold symmetric diffraction patterns, with *pq* indices governed by the irrational number $2+\sqrt{3}$ (Janssen *et al.*, 2007). Penrose tilings have fivefold rotation symmetry and have diffraction patterns with sharp peaks whose indices are governed by the number $2+\sqrt{5}$, which is twice the golden mean. In this sense, our tilings of squares and equilateral triangles, built by recursive isomorphic substitutions of a simple motif, constitute a simple type of quasiperiodic space-filling plane structure with interesting diffraction patterns with fractal-like properties.

Square–triangle tilings provide a basis for systematic description of the structures of some Frank–Kasper intermetallic phases (Frank & Kasper, 1959; Sullivan, 2000). Thus 4^4 corresponds to the cubic *A*15 structure, 3^6 to the hexagonal *Z* structure and $3^2.4.3.4$ to the tetragonal σ-phase structure. In these structures space is divided into tetrahedra ('tetrahedrally close packed'). The dual structures are simple tilings and are those of the well known types I, III and IV clathrate structures, respectively. Interestingly these occur in a number of contexts in soft matter. Of particular interest in connection with this work is that related dodecagonal quasicrystals based on square–triangle tilings have recently been found in supramolecular liquid crystals (Ungar & Zeng, 2005), in *ABC* star (tri-block) polymers (Hayashida *et al.*, 2007) and in colloidal assemblies of inorganic nanoparticles (Talapin *et al.*, 2009).

This work was supported by the US National Science Foundation (grant number DMR 0804828). Acknowledgment is made to the Donors of the American Chemical Society Petroleum Research Fund for partial support of this research.

References

Frank, F. C. & Kasper, J. S. (1959). *Acta Cryst.* **12**, 483–499.
Gähler, F. & Klitzing, R. (1997). *The Mathematics of Long-Range Aperiodic Order*, edited by R. V. Moody. Dordrecht: Kluwer Academic Publishers.
Hayashida, K., Dotera, T., Takano, A. & Matsushita, Y. (2007). *Phys. Rev. Lett.* **98**, 195502.
Hermisson, J., Richard, C. & Baake, M. (1997). *J. Phys. I France*, **7**, 1003–1018.
Janssen, T., Chapuis, G. & de Boisseau, M. (2007). *Aperiodic Crystals.* Oxford University Press.
Leung, P. W., Henley, C. L. & Chester, G. V. (1988). *Phys. Rev. B*, **39**, 446–458.
O'Keeffe, M. & Hyde, B. G. (1980). *Philos. Trans. R. Soc. London Ser. A*, **295**, 553–623.
O'Keeffe, M., Peskov, M. A., Ramsden, S. J. & Yaghi, O. M. (2008). *Acc. Chem. Res.* **41**, 1782–1789.
Stampfli, P. (1986). *Helv. Phys. Acta*, **59**, 1260–1263.
Sullivan, J. M. (2000). *Proceedings of the Third EuroConference on Foams, Emulsions and their Applications (Eurofoam 2000)*, pp. 111–119. Bremen: Verlag MIT.
Talapin, D. V., Shevchenko, E. V., Bodnarchuk, M. I., Ye, X., Chen, J. & Murray, C. B. (2009). *Nature (London)*, **462**, 964–967.
Ungar, G. & Zeng, X. (2005). *Soft Matter*, **1**, 95–106.
Zeng, X. & Ungar, G. (2006). *Philos. Mag.* **86**, 1093–1103.